Robotic Farming System Using Collaborative UAV and UGV

Feng-Chun Tai, Yen-Jung Kuo, and Ching-Chih Tsai, *Fellow, RST*

***Abstract*—This paper presents a collaborative farming operation system composed of an outdoor unmanned aerial vehicle (UAV), which is a quadrotor, and an unmanned ground robot (UGV) with a tracked mobile platform. Both UAV and UGV are connected by an electric cable that lets the UAV extend the working time in the farm field. In order to execute the farming missions, a path planning algorithm is applied to generate a feasible path with some restrictions of both UAV and the UGV. A trajectory tracking control with input constraints is proposed and implemented to track the designed path from the path planning algorithm. Simulations and experimental results are well used to show the effectiveness of the two proposed methods by analyzing their output results.**

***Index Terms*—path planning, trajectory tracking control, nonlinear control, unmanned aerial vehicle (UAV), unmanned grounded vehicle (UGV).**

I. Introduction

COOPERATIVE operations of autonomous ground robots and drones have become popular for various applications such as warehouse system, navigating system, farming system, military, and so on. The UAV has the merits of overcoming complex terrain and nice vision on top but has the disadvantages of low power storage and low loading weights. The authors in [1] showed that the segmentation technique attached on the UAV had an ability to monitor the condition of grass in a farm. On the contrary, the UGV is able to carry large loading weight and a battery with large storage but is limited to move on relatively flat terrains. The collaborative system that composes of two kind of vehicles could take the merits of each other. Thus, much research and investigation have been conducted to construct such collaborative systems. The studies in [2]-[3] reported successful applications of such collaborative robot systems. The authors in [2] showed that the UAV safely took off from the UGV, tracked the UGV in the air and landed on the top platform of the UGV for charging, while the authors in [3] adopted a tether connecting with the UAV and UGV, and set up a fulcrum such that the UAV could pull the tether cross the fulcrum helping the UGV to climb the cliff.

The research about path planning is pretty rich. It is an importance issue that robots need to automatically search a collision-free path, complete the tasks and optimize their path with some specific restrictions. Generally, the path planning method can be separated into two classifications: graph search methods and geometric methods. One of the methods belonging to the classification of graph search is a well-known algorithm in [4]-[5], which generated the shortest path. On the other hand, the geometric methods are inspired by the original geometric patterns such as circle, line and arcs to find feasible paths. The authors in [6] generated the Bezier curve path including obstacle avoidance for a mobile vehicle in real-time. In addition, the trajectory control, path planning and navigation of wheeled or tracked mobile platforms were referred to [7]-[11].

Inspired by the aforementioned studies, this paper aims to integrate a new path planning algorithm and a constrained trajectory tracking controller to carry out the collaborative missions in a farm field. In order to extend the operation time of the UAV, there is a power cable connecting with the UAV and UGV. The UGV carries a battery with the large storage capacity to provide required power to the UAV. Because the power cable will droop under the influence of the gravity and cause the damage to the plants, it is necessary to model the drooping cable to ensure that it will not contact the tip of the plants. With the restriction of the cable length, the path planning algorithm is applied to generate a proper path for both robots. To ensure the well-covered working area in the field during the farming missions, the Boustrophedon path is chosen for the UAV. Once the path has been produced, the nonlinear trajectory tracking controller will be proposed to track desired paths and accomplish desired farm missions.

The rest of this paper is outlined as follows. The overall system structures are described in Section II. Section III and IV respectively describe the path planning algorithm and trajectory tracking control with input constraints. Section V presents the simulation results of two proposed methods and analyzes them using MATLAB. Section VI conducts and discusses the experimental results. Section VII states the conclusions and future work of the paper.

II. System Description

This section is aimed to describe the system structure of the proposed system and system configurations of the UGV and UGV. This collaborative system can be used for air surveys, pesticide spraying and plant condition maintenance. Fig. 1 shows the proposed collaborative farming system, where one UAV, AR Drone 2.0, is equipped with the control board, Arduino Nano, and Bluetooth 4.0 module, and one UGA is a tracked mobile robot carrying large batteries, a set of iBeacon devices and one RealSense camera. The iBeacon module using Bluetooth is employed to find the current position of the UGV using the measurements of RSSI values and least squares method when the robotic farming system works for indoor apparatus or protected agriculture. The RealSense camera is used to find features surrounding the working space and proceed with moving path planning if autonomous navigation is needed for the UGV used in a tomato planting field with facility of protected agriculture.

Feng-Chun Tai, Yen-Jung Kuo, and Ching-Chih Tsai are with the Department of Electrical Engineering, National Chung Hsing University, Taichung 40227, Taiwan.
(Corresponding author Ching-Chih Tsai, email: cctsai@nchu.edu.tw) (email: fctai@nchu.edu.tw, g107064034@mail.nchu.edu.tw)

The authors deeply acknowledge financial support from Ministry of Science and Technology (MOST), Taiwan, ROC, under contract MOST 107-2221-E-005-073-MY2.

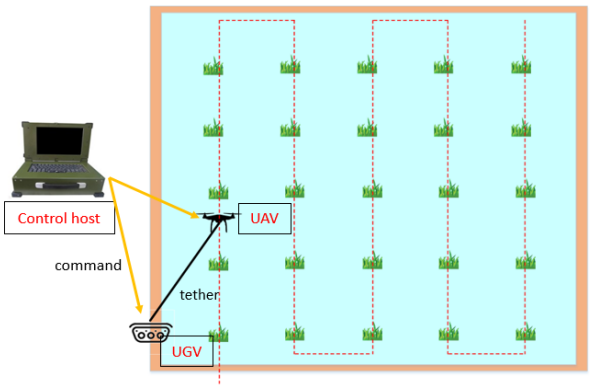

Fig. 1. Illustration of the proposed farming system using collaborative UAV and UGV.

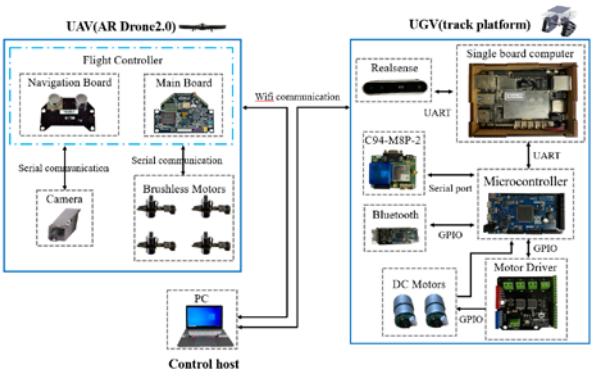

Fig. 2. System structure.

To increase extra loading weights, we removed the battery on the UAV to provide more space for the control board, and added a cable to connect the UAV to the UGV, thus delivering the power of the UAV from the UGV. Note that there is no battery on the UAV, and a large storage battery is mounted on the UGV in order to provide the main power for each UAV and UGV. Both UAV and UGV are remotely commanded by a host computer which is a personal computer (PC). Fig. 2 depicts detailed system structure of the robotic faming system.

III. Path Planning

This section is dedicated to describe a revised Boustrophedon path planning algorithm to generate a desired path for both UAV and the UGV. It is necessary that the UAV maintains a constant speed flying through the farm to ensure the well-distributed survey and spraying range in such air surveys and pesticide spraying missions, and the UGV needs to follow the UAV so as to provide power or pesticide for the UAV. Since there is a cable connecting with both robots for power supply, two robots must be held in a tolerant distance preventing the cable from being broken or interfering the poses of both robots. By modeling the hanging cable, the tolerant length can be obtained and the tolerant distance between the UAV and the UGV in farm field can be ensured. The UGV is limited to move only on the ridge of the farm field. The purpose of this algorithm is to consider the limitations that have been aforementioned and to find the feasible path for both UAV and UGV.

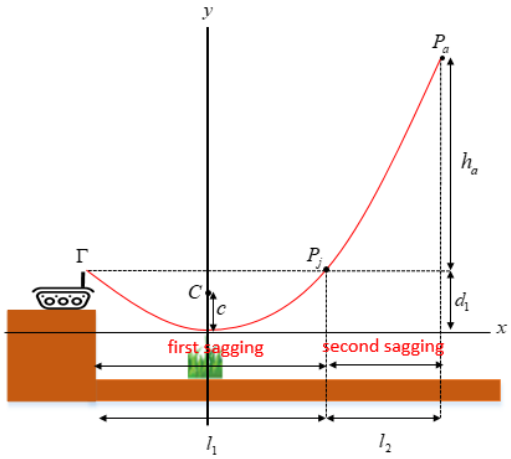

Fig. 3. Parabola model.

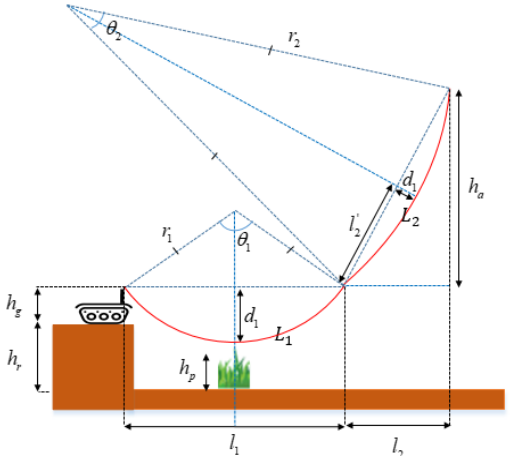

Fig. 4. Cable length calculation model.

A. Cable Separation

In the subsection, we model the hanging cable to find the tolerant length. Since the hanging cable is not an idea catenary, it is required to separate the cable into two sagging parts and use the parabola approach to gaining the position of the first and second sagging points. The side view of the parabola cable modeling is shown Fig. 3, where P_j is the position of junction between the first and second sagging points and P_a is the position of the UAV. Furthermore, d_1 is the first sagging degree, C is the focus and c is the distance between C and the origin, h_a is the height of UAV with respect to the top of the UGV, l_1 and l_2 are the projection of the first and second sagging to the ground, respectively. l_s denotes the sum of two projections and equals the 2D distance between the UAV and the UGV. We have the parabola function Γ: $x^2=4cy$ and substitute it by $P_j(l_1/2, d)$ and $P_a(l_s - l_1/2, h_a + d)$ expressed by

$$\left(\frac{l_1}{2}\right)^2 = 4cd \tag{1}$$

$$\left(l_{all} - \frac{l_1}{2}\right)^2 = 4c\left(h_a + d\right) \tag{2}$$

Then, find l_1, which is the solution of (1) and (2) as below.

$$\left(\frac{l_1}{2}\right)^2 \Big/ \left(l_s - \frac{l_1}{2}\right)^2 = \frac{d}{h_a + d} \tag{3}$$

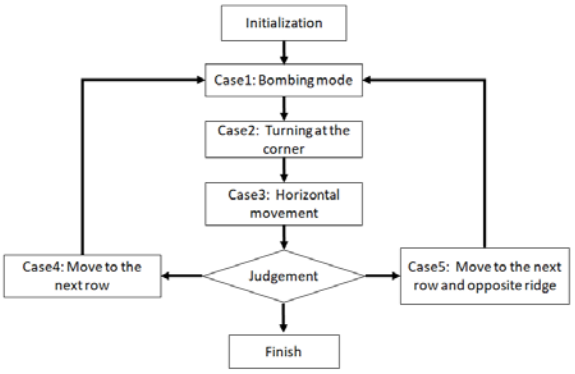

Fig. 5. Flow chart of the proposed constrained path planning algorithm.

$$h_a/4 \cdot l_1^2 + l_s l_1 d - d \cdot l_s^2 = 0 \tag{4}$$

B. Hanging Cable Model

The first and second sagging cable is described as the circle arcs with different radius of r_1 and r_2. For the position of junction between the first and second sagging points has been found, the cable model is depicted as in Fig. 4. The lengths of the first and second parts of the sagging cable, L_1 and L_2, are calculated by the following equation.

$$\begin{aligned} &(r_1 - d_1)^2 + \left(l_1/2\right)^2 = r_1^2 && l_2' = 1/2\left(h_a^2 + l_2^2\right)^{1/2} \\ &r_1 = \frac{1}{2d_1}\left(d_1^2 + \left(l_1/2\right)^2\right) && (r_2 - d_2)^2 + l_2'^2 = r_2^2 \\ & && r_2 = \left(d_2^{\,2} + l_2'^{\,2}\right)/2d_2 \\ &\theta_1 = 2\sin^{-1}\left(l_1/2r_1\right) && \theta_2 = 2\sin^{-1}\left(l_2'/r_2\right) \\ &L_1 = 2\pi r_1\theta_1 && L_2 = 2\pi r_2\theta_2 \end{aligned} \tag{5}$$

where h_g is the height of the UGV, h_r is the height of farm ridge, h_p is the height of plant, d_1 and d_2 are the sagging degree of first and second parts of sagging cable, respectively, θ_1 and θ_2 are the angle of arc of first and second parts of the sagging cable, respectively. It implies that the total power cable is L_{sum}=L_1+L_2. Once the cable has been pulled tight, it provides additional running range that the UAV and UGV have to keep with each other. The tolerant distance is described as below.

$$L_t = L_{sum} - \sqrt{(l_1 + l_2)^2 + h_a^{\,2}} \tag{6}$$

It is impossible to maintain a certain distance between two robots during the whole farm missions because the velocity curves or magnitude of acceleration are different from each other. The tolerant distance gives the buffer to cancel the distance difference occurred by accelerating or decelerating on the UAV and the UGV.

C. Revised Boustrophedon Path Planning Algorithm

Once the model of power cable and tolerant length has been obtained, the 3D modeling of the UAV and the UGV can be established in the farm field. The primary ideas of this algorithm are to let the UAV keep fly at a current speed when it passes through the farm field in the Boustrophedon path. The UGV must follow the UAV and moves only on the ridge with a tolerant distance by the tolerant length L_t for power supply. The flow chart of the path planning algorithm is elaborated in Fig. 5. In the initialization stage, both UAV and UGV get started at the respective starting points outside the farm field with a distance L_{sum} and ready to go the next stage.

The UGV will be the first one getting into the field. The entire algorithm is divided into 5 general cases and one judgment.

Case 1: Bombing Mode

In order to have a current speed during the mission procedure in the field, the UAV and UGV start up with a respective acceleration and keep at the same current speed to maintain a fixed distance. Two robots move along a straight line through the field, and the UAV is able to execute a desired mission. The velocity profiles use the trapezoid velocity profiles on both robots. When the UGV is closed to the angle with a braking distance, it is the cast point that both UAV and UGV go to the next case.

Case 2: Turn at the Corner

In this case, since the UGV is moving to the corner and about to turn 90 degrees, the preset velocity is no longer required on the UAV and UGV. After entering in this case, the UGV executes the velocity planning which decelerates, spins 90 degrees, accelerates and keeping at the preset velocity. This multi-trapezoid velocity program will let the UGV move to the horizontal ridge. On the other side, the UAV is going to hold in a proper position with the default cable length L_{sum} when the UGV is moving to the nearest point to it on horizontal ridge. The velocity planning of the UAV will decelerate, keep at the preset velocity and then decelerate to move back to the desired proper position. If the UGV move to the nearest point to the UAV when the UAV is holding at the proper position, it is the cast point that two robots go to the next case.

Case 3: Horizontal Movement

In the beginning of this case, the total cost time is obtained by calculating the spending time that the UAV moves to the horizontal ridge in the preset velocity. During the preset velocity stage, the UAV can continue the farm mission. The total cost time is the input of the trapezoid velocity program including movement in the preset velocity and deceleration to stop on the UGV. The jump point in this case is that when the UAV flies out from the field.

Case 4: Move to the Next Row

The general motion of the UGV in this case are to move horizontally to the corner in Case 2, spin and go into the straight ridge in Case 1. On the other hand, the UAV will be kept at a certain distance between the UGV and UAV, and fly with a shape of a half playground to get into the next row. The relative position between two robots is described as follows;

$$\begin{aligned} &C_g : (x - x_g)^2 + (y - y_g)^2 - l_s^2 \\ &L_{rd} : x_{rd} - x \\ &L_{rn} : x_{rn} - x \end{aligned} \tag{7}$$

where the $P_{ugv}(x_g, y_g)$ is the current position of the UGV. The position of the UAV must be the solution of the circle function C_g. Then, we generate two line functions L_{rd} and L_{rn} which are the current row and the next row. Find the solution points by

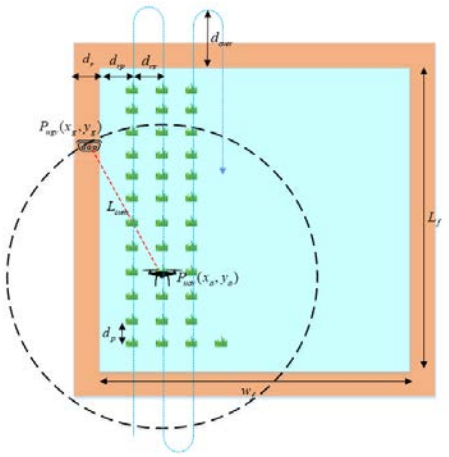

Fig. 6. The sketch map.

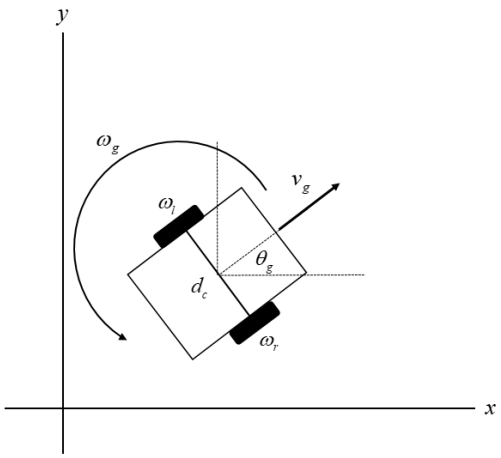

Fig. 7. UGV structure.

three equations. With respect to the last position of the UAV, the nearest point is the next moving point.

Similar to Case 3, there is a total cost time which is the spending time coming from the trapezoid velocity program on the UGV. At the final stage, both UAV and UGV will prepare to move with a preprogrammed velocity which means that it is time to go to Case 1.

Case 5: Move to the Next Row and Opposite Ridge

This case is similar to Case 4. The only difference is that the UGV has to move to the opposite straight ridge to maintain the default cable length L_{sum} once the UAV has finished half number of the rows.

Judgement:

In this judgement stage, the main determination factor is the number of the rows that the UAV has run. If the UAV has finished the half number of the rows, Case 5 will be the next stage. The reverse is Case 4. Once the UAV has run all over the rows, the whole algorithm is completed.

In general, both UAV and UGV are kept in the default distance generating by the cable length L_{sum}. If there are some conditions occurred, two robots will still be in the extended range offered from the tolerant length L_t. The main ideas of this path planning algorithm is sketched in Fig. 6, where the $P_{ugv}(x_g, y_g)$ and $P_{uav}(x_a, y_a)$ are respectively the positions of the UGV and UAV, w_f and L_f are the width and length of the field, d_r is the width of the ridge, d_{rp} is the width of the first row to ridge, d_{rtr} is the interval of rows, d_{over} is the distance of the UAV running over the field, and d_p is the interval of the plants.

IV. Trajectory Tracking Control with Input Constraints

This section will design a constrained tracking controller implementing on the UGV to track the paths generated by the path planning algorithm. The idea of this nonlinear control method is to consider the velocity constraints of the driving motor and show the constrained nonlinear controller to be asymptotically stable when time goes to infinity.

A. Revise Boustrophedon Path Planning Algorithm

The overview of the UGV structure is shown in Fig. 7. With the overview, we drive a kinematic model of a differential mobile robot with two velocity-controlled wheels as below.

$$S(q) = \begin{bmatrix} \cos\theta_g & 0 \\ \sin\theta_g & 0 \\ 0 & 1 \end{bmatrix} \tag{10}$$

The kinematic path tracking control problem is to find a local trajectory tracking control law with speed constraints so that the UGV can asymptotically follow the desired moving trajectories expressed by

$$\dot{q}_r = S(q_r) \cdot \mu_r \tag{11}$$

where $q_r(t)=[x_r\ y_r\ \theta_{gr}]^T$ and $\mu_r=[v_{gr}\ \omega_{gr}]^T$. We define the errors between the actual and desired postures $\tilde{x}$, $\tilde{y}$, $\tilde{\theta}_g$ as

$$\tilde{x} = x_r - x \quad \tilde{y} = y_r - y \quad \tilde{\theta} = \theta_{gr} - \theta_g \tag{12}$$

With these defined errors, the tangential error $e_1(t)$, the normal error $e_2(t)$ and the orientation error $e_3(t)$ can be found via the subsequent matrix

$$\begin{bmatrix} e_1(t) \\ e_2(t) \\ e_3(t) \end{bmatrix} = \begin{bmatrix} \cos\tilde{\theta} & \sin\tilde{\theta} & 0 \\ -\sin\tilde{\theta} & \cos\tilde{\theta} & 0 \\ 0 & 0 & 1 \end{bmatrix} \begin{bmatrix} \tilde{x} \\ \tilde{y} \\ \tilde{\theta} \end{bmatrix} \tag{13}$$

Differentiating the errors with respect to time obtains

$$\begin{aligned} \dot{e}_1 &= \omega_g e_2 - v_g + v_{gr}\cos e_3 \\ \dot{e}_2 &= -\omega_g e_1 + v_{gr}\sin e_3 \\ \dot{e}_3 &= \omega_{gr} - \omega_g \end{aligned} \tag{14}$$

B. Control laws with Speed Constraints

Notice that all the transformed errors, $e_1(t)$, $e_2(t)$ and $e_3(t)$, are continuous and bounded, the original errors, $\tilde{x}$, $\tilde{y}$, $\tilde{\theta}$, are bounded and continuous. This means that when $e_1(t)$, $e_2(t)$ and $e_3(t)$ approach zero when times goes to infinity, it follows that $\tilde{x}(t)$, $\tilde{y}(t)$, $\tilde{\theta}(t)$ approach to zero when time goes to infinity, namely that

$$\lim_{t\to\infty} e_1(t) = 0, \lim_{t\to\infty} e_2(t) = 0, \lim_{t\to\infty} e_3(t) = 0$$

if and only if $\lim_{t\to\infty} \tilde{x}(t) = 0, \lim_{t\to\infty} \tilde{y}(t) = 0, \lim_{t\to\infty} \tilde{\theta}(t) = 0$.

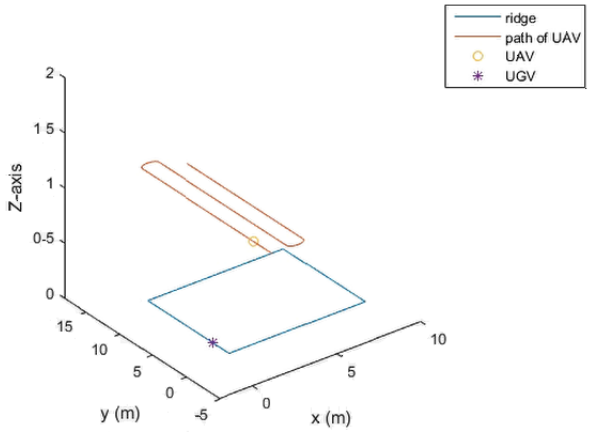

Fig. 8. Case 1: Bombing mode.

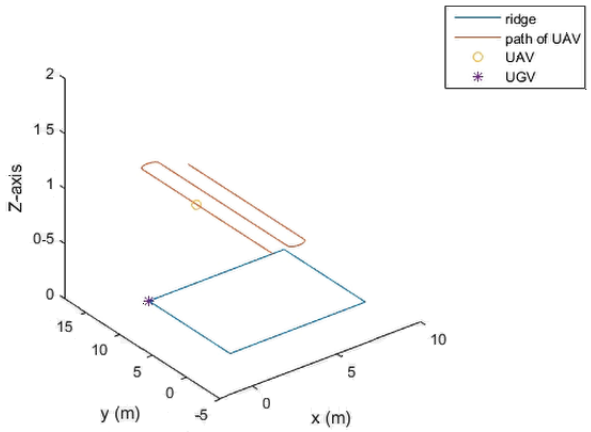

Fig. 9. Case 2: Turn at the corner.

To stabilize the system (14), the control laws of v_g and ω_g are proposed as follows;

$$\begin{aligned} v_g &= sat(k_1 e_1 + v_{gr}\cos e_3), k_1 > 0 \\ \omega_g &= sat(\omega_{gr} + k_2 v_{gr} e_2 + k_3 v_{gr}\sin e_3), k_2 > 0, k_3 > 0 \end{aligned} \tag{15}$$

such that the closed-loop error system becomes

$$\begin{aligned} \dot{e}_1 &= -k_1 e_1 + \omega_g e_2 \\ \dot{e}_2 &= -\omega_g e_1 + v_{gr}\sin e_3 \\ \dot{e}_3 &= -k_2 v_{gr} e_2 - k_3 v_{gr}\sin e_3 \end{aligned} \tag{16}$$

Consequently, the speed commands of the right and the left driving wheels are obtained from $\omega_r = d_c\omega + (v_g R/2)$ and $\omega_l = -d_c\omega + (v_g R/2)$, respectively.

C. Lyapunov Stability

To show the local asymptotical stability of the closed-loop error systems, we find the following Lyapunov function candidate and consider the error trajectories nearby the origin

$$V = \tfrac{1}{2}\left(e_1^2 + e_2^2\right) + \left(1 - \cos e_3\right)/k_2 \tag{17}$$

Taking the time derivative of V along its trajectory gives

$$\begin{aligned} \dot{V} &= e_1\dot{e}_1 + e_2\dot{e}_2 + \dot{e}_3\sin e_3 / k_2 \\ &= -k_1 e_1^2 - k_3 v_{gr}\sin^2 e_3 / k_2 \le 0 \end{aligned} \tag{18}$$

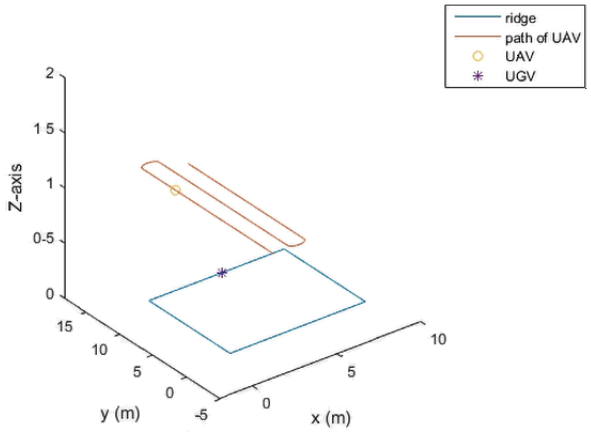

Fig. 10. Case 3: Horizontal movement.

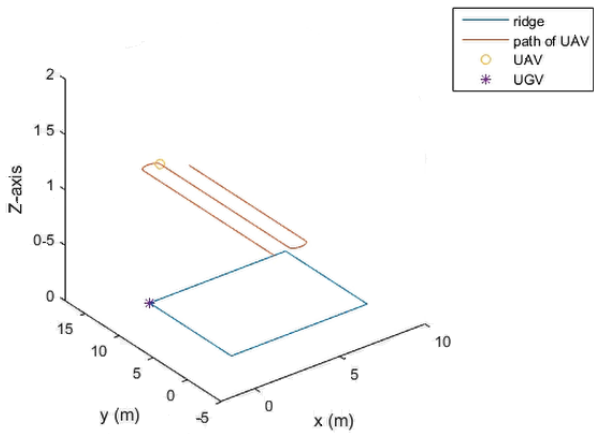

Fig. 11. Case 4: Move to the next row.

Definitely, V is semi-negative definite. According to Barbalat's lemma and the Lasalle's invariance principle, if v_{gr} is positive and nonzero, then $e_1(t)$ and $e_3(t)$ approach zero as time goes to infinity, i.e., $\lim_{t\to\infty} e_1(t) = 0$ and $\lim_{t\to\infty} e_3(t) = 0$.

From (17) and (18), if follows that $e_2(t) \in L_2$ and $e_2(t)$ are continuous and bounded and $\lim_{t\to\infty} \dot{e}_2(t) = 0$, this implies that $\lim_{t\to\infty} e_2(t) = 0$. Finally, we prove that $e_1(t)$, $e_2(t)$ and $e_3(t)$ approach zero asymptotically. From (13), and it follows that $\tilde{x}(t)$, $\tilde{y}(t)$, $\tilde{\theta}(t)$ must locally approach zero when t→∞.

V. Simulation Results and Discussion

This section provides two illustrative scenarios to explore the effectiveness and superiority of our proposed path planning algorithm and trajectory tracking controller executing in discrete time. Both examples are simulated by using MATLAB with units of meter and degree. In the first example, we initialize the power cable model by setting d_1=0.35, h_a=1 and l_s=4. The projection of the first sagging to the ground can be calculated by l_1=0.879. Next, we input the further information, d_1=0.15, h_g=0.3 and h_r=0.3, thus finding that the total length of the power cable is L_{sum}=4.4793. This implies that the tolerant length is L_t=0.1131. Finally, we establish the information of the farm field by setting w_f=8, L_f=12, d_r=1, d_{rp}=1, d_{rtr}=1, and d_p=1.

Figs. 8-11 show the simulation results of the proposed path planning algorithm that generates the trajectory path for both UAV and UGV. The blue line in the figure denotes the ridge of

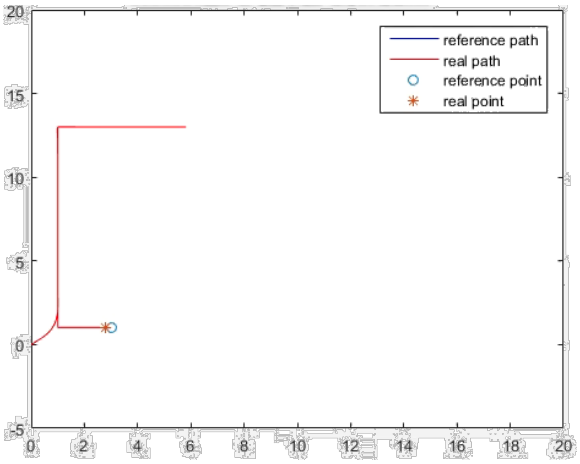

Fig. 12. Simulation result of trajectory tracking.

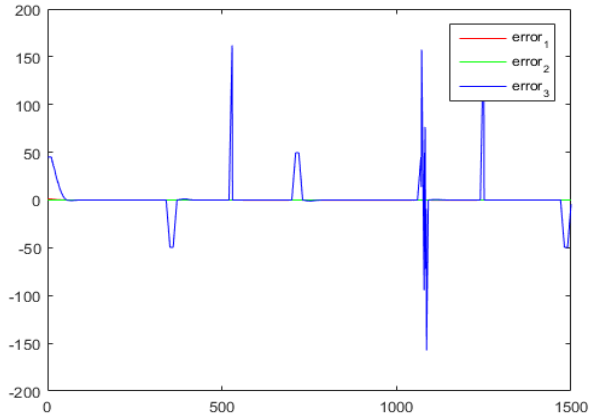

Fig. 13. Simulation result of the tracking errors (e_x, e_y, e_{theta}).

the farm and the orange line represents the Boustrophedon path that the UAV executes. The circle and star icon represent the current positions of the UAV and UGV, respectively. In any cast time, two robots are keeping in the tolerant range.

The second simulation is carried out to show the effectiveness of the proposed constrained trajectory tracking controller mounting on the UGV. The parameters of the controller are decided by k_1=4, k_2=8 and k_3=4. The reference path is given by the path planning algorithm we have aforementioned. The current speed and acceleration are set by 0.4 m/sec and 0.1 m/sec^2. Fig. 12 shows the tracking results by using the trajectory tracking controller on the UGV. The red line denotes the tracking path which is almost overlapping the reference path, which means that the tracking controller is well effective. Fig. 13 depicts the simulations results of three errors, the tangential error $e_1(t)$, the normal error $e_2(t)$ and the orientation error $e_3(t)$, during the whole tracking procedure. Both tangential and normal errors approach zero in a little time which implies the merits of the proposed trajectory tracking method. The orientation error below 50 degrees occurred at the time when UGV moved to the corner and turns 90 degrees. On the contrary, the orientation errors exceeding 50 degrees are caused by the isometric angle. It means that it has no influence during the tracking phase.

VI. Experimental Results and Discussion

This section conducts two experiments to examine the applicability of our proposed trajectory tracking controller with path planning algorithm executing in an indoor facility agriculture environment. In order to obtain the tracking errors

Fig. 14. Appearances of the experimental UGV and UAV.

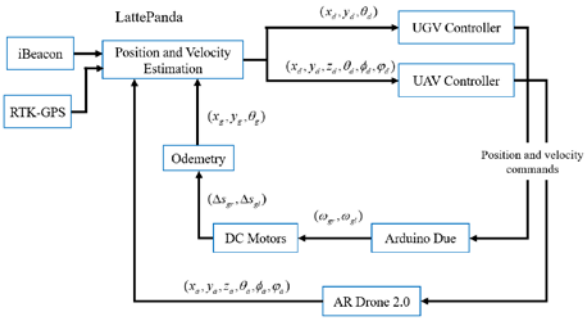

Fig. 15. Block diagram of the overall control system.

during the real-time experiments, we fused the odometry and iBeacon (indoor localization with Bluetooth module) or RTK-GPS (outdoor localization) as the internal localization method and installed the laser beam on the robot, in order to point to the ground as the external scaler. Fig.14 shows the setup of both experimental platforms, and Fig. 15 depicts the control block diagram of the whole system.

The first experiment is carried out to show the performance of the UGV to move along our designed farming environment. The experimental farming environment is overviewed in Fig. 16, where its size information is displayed. Fig. 17 depicts the trajectory tracking result of the proposed method in which the L shape path was generated by the farming path planning algorithm in Fig. 12. The current velocity was set at 0.4 m/sec and the velocity and angular speed was planned by using the trapezoid curve velocity programing. The results in Fig. 17 indicate the proposed nonlinear control method effectively steered the UGV to move along the planned path via the farming path planning algorithm.

The second experiment is conducted to show the trajectory tracking performance of the UAV. The results in Fig. 18 reveal that the UAV followed the path generated by the proposed path planning algorithm. The third experiment is performed to demonstrate the proposed collaborative farming robot system, which are composed of an UAV and an UGV with a differential tracked mobile platform. The proposed path planning algorithm was applied to generate the feasible path for both UAV and UGV with the restriction of power cable and collaborative formation. As the result in Fig. 19, both robots steadily moved

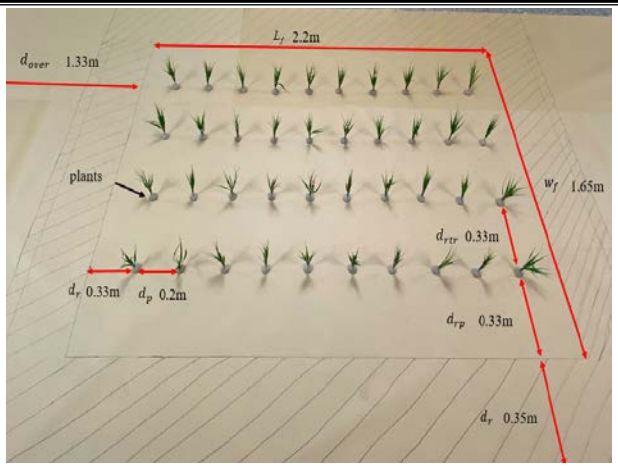

Fig. 16. Schematics of the experimental farming environment.

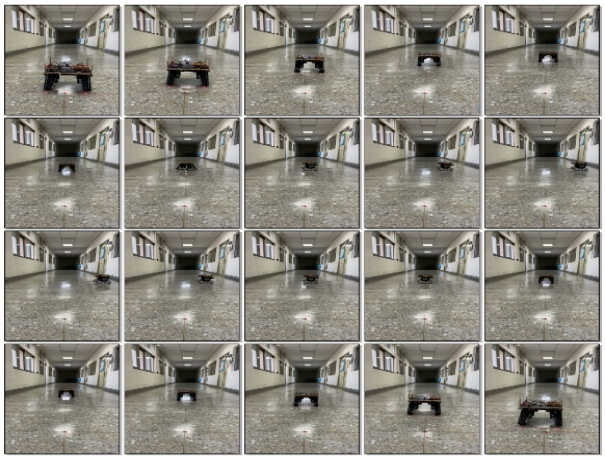

Fig. 17. Experimental pictures of tracking result of the L-shape path trajectory.

along the farming field without interfering the poses of each other, which thus verified the effectiveness of the proposed method.

VII. Conclusions

This paper has presented a collaborative robotic farm system using one UAV which is a quadrotor, and one UGV which is a tracked mobile platform. The overall system structure has been designed, and the main research methods, including the proposed path planning algorithm and constrained trajectory tracking law, have been proposed for such a farming system. Through simulation and experimental results, both methods have been shown effective in planning and controlling movements of both UAV and UGV. Future work will be conducting more experiments to show the effectiveness of the proposed robotic farm system in a real farm.

Fig. 18. Still pictures of trajectory tracking of the UAV.

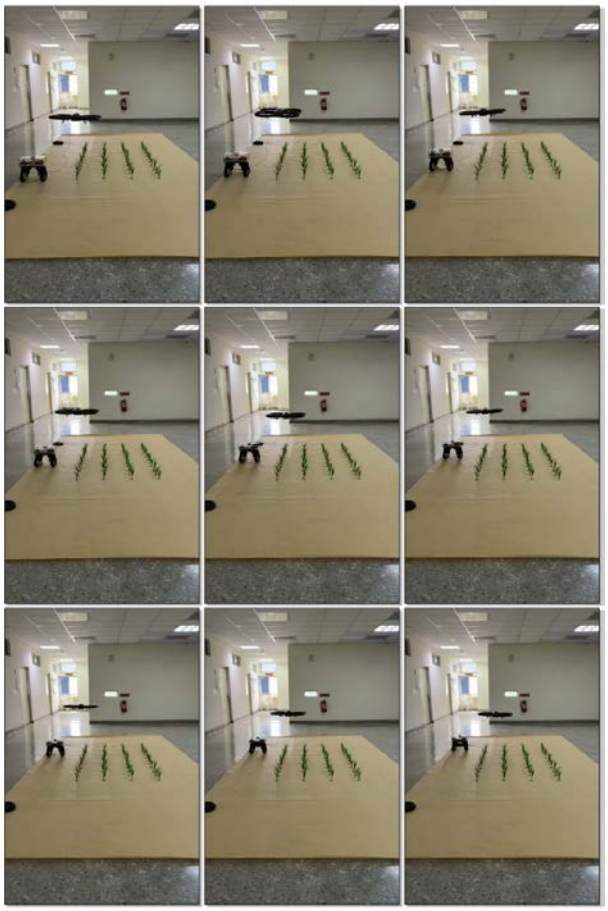

Fig. 19. Still pictures of trajectory tracking of the

References

[1] S. Tsuichihara, S. Akita, R. Ike, M. Shigeta, H. Takemura, T. Natori, K. Shindo, Y. Ide, and S. Tejima, "Drone and GPS sensors-based grassland management using deep-learning image segmentation," in *Proc. of* 3rd *IEEE Intern.Conf. on Robotic Computing*, 2019.

[2] J. K. Lee, H. Jung, H. Hu, and D. H. Kim," Collaborative control of UAV/UGV," in *Proc. of the 11th Intern.Conf. on Ubiquitous Robots and Ambient Intelligence*, Malaysia, 2014.

[3] M. Takahiro, P. Khrapchenkov, and H. Koichi, "UAV/UGV Autonomous Cooperation: UAV assists UGV to climb a cliff by attaching a tether," in *Proc. of 2019 IEEE International Conference on Robotics and Automation(ICRA)*, Canada, Montreal, May 20-24, 2019

[4] P.E. Hart, N.J. Nilsson, and B. Raphael. "A formal basis for the heuristic determination of minimum-cost paths," *IEEE Transactions on Systems Science and Cybernetics*, vol. 2, no. 2, 1968.

[5] R. Zhou and E. Hansen. "Multiple sequence alignment using anytime A*," *In Proc. of the 18th National Conference on Artificial Intelligence*, 2002.

[6] L. Ma, J. Yang, and M. Zhang, "A two-level path planning method for on-road autonomous driving," in *Proc. of the International Conference on Intelligent Systems Design and Engineering Application*, 2012.

[7] J. L. Pang, *Nonlinear control of a wheeled mobile robot using polar coordinate*, M.S. thesis, Department of Electrical Engineering, National Chung Hsing University, pp. 27-46, July 2004.

[8] M. Sahmoudi and R. Landry, "A nonlinear filtering approach for robust multi-GNSS positioning in presence of multipath and ionospheric delays," *IEEE Journal of Selected Topics in Signal Processing*, 2009.

[9] Y. Kanayama and N. Miyake, "Trajectory generation for mobile robots," in *Proc. of* the *International Symposium on Robotics Research*, pp. 16-23,

1985.
[10] Y. L. Chiu, *Fuzzy reactive and hybrid navigation of a special-purpose service robot*, M.S. thesis, Department of Electrical Engineering, National Chung Hsing University, July 2002.
[11] C. C. Lai, *Outdoor localization and reactive control of an autonomous mobile robot*, M.S. thesis, Department of Electrical Engineering, National Chung Hsing University, July 1999.

Feng-Chun Tai received the B.S., M.S. and Ph.D. degrees in Department of Electrical Engineering from National Chung Hsing University, Taichung, Taiwan, ROC. in 2007, 2010 and 2018, respectively. His current research interests include mobile robots, intelligent control, navigation system and their applications to industrial processes and machines.

Yen-Jung Kuo received the M.S. degree in Department of Electrical Engineering from National Chung Hsing University, Taichung, Taiwan, ROC. in 2020, respectively. His current research interests include intelligent control and formation control.

Ching-Chih Tsai received the Diplomat in Electrical Engineering from National Taipei Institute of Technology, Taipei, Taiwan, ROC, the MS degree in Control Engineering from National Chiao Tung University, Hsinchu, Taiwan, and the Ph.D degree in Electrical Engineering from Northwestern University, Evanston, IL, USA, in 1981, 1986 and 1991, respectively. Currently, he is currently a Life Distinguished Professor in the Department of Electrical Engineering, National Chung-Hsing University, Taichung, Taiwan, where he served the Chairman in the Department of Electrical Engineering from 2012 to 2014. Since August, 2019, he has also served the Vice Dean of the R&D Office, NCHU. He is a Fellow of IEEE, IET, CACS, and RST.

Prof. Tsai served as the Chair, Taipei Chapter, IEEE Control Systems Society, from 2000 to 2003, and the Chair, Taipei Chapter, IEEE Robotics and Automation Society from 2005 to 2006. In 2007, he was the program chair of 2007 CACS international automatic conference sponsored by Taipei chapter, IEEE control systems society. In 2010, he served as the program co-chair of SICE 2010 annual conference in Taiwan, which was technically sponsored by IEEE CSS; in 2011, he served as the General Chair, 2011 International conference on service and interactive robotics; in 2012, he has served as the General Chair, 2012 International conference on Fuzzy Theory and Its Applications, the General Chair, 2012-2015 CACS International Automatic Control Conferences, and the General Chair, 2016-2019 International Conference on Advanced Robotics and Intelligent Systems. Dr. Tsai served the two-term President, Chinese Institute of Engineers in Central Taiwan, Taiwan from 2007 to 2011, two-term President of Chinese Automatic Control Society from 2012 to 2015, and two-term President of Robotics Society of Taiwan form 2016 to 2019. Dr. Tsai also served as a steering committee of Asian Control Association from 2014 to 2019, and a BOG member of the IEEE SMCS from 2017 to 2019, a Vice President of International Fuzzy Systems Association from 2015 to 2019. Furthermore, he has been the Executive Directors in Boards of Government of thee professional associations, including Robotic Society of Taiwan, Taiwan Fuzzy Systems Association, and Taiwan Systems Association since 2009, the Chair, Taichung Chapter, IEEE Systems, Man, and Cybernetics Society since 2009, the Chair of IEEE SMC Technical Committee on intelligent learning in control systems since 2009, a BOG member of IEEE Nanotechnology council since 2012, and the President-Elect of International Fuzzy Systems Association since 2019.

Dr. Tsai has published more than 550 technical papers, and seven patents in the fields of control theory, systems technology and applications. Dr. Tsai is respectively the recipients of the Third Society Prize Paper Award from IEEE Industry Application Society in 1998, the Outstanding Automatic Control Engineering Award in 2008 from Chinese Automatic Control Society (CACS), and the Outstanding Engineering Professor Award in 2009 from the Chinese Institute of Engineers in 2009, the IEEE Most Active SMC Technical Committee (TC) Award in 2012 from IEEE SMC Society, the Outstanding Electrical Engineering Professor Award from the Chinese Institute of Electrical Engineering in 2014, Outstanding Industry Contribution Award from Taiwan Systems Association in 2016, and many best paper awards from many international conferences technically supported by IEEE, and the outstanding research award from the Ministry of Science and Technology (MOST), Taiwan, in 2018. He is the advisor, IEEE SMC student branch chapter at National Chung Hsing University; this chapter was the recipient of certificate of appreciation from IEEE SMCS in 2009. He has served as the associate editors of International Journal of Fuzzy Systems, and IEEE Transactions on Systems, Man and Cybernetics: Systems, IEEE Transactions on Industry Informatics, and International Journal of Electrical Engineering. Recently, he has served as the Editor in Chief of a new international robotics journal called “iRobotics”. His current interests include advanced nonlinear control methods, deep model predictive control, fuzzy control, neural-network control, advanced mobile robotics, intelligent service robotics, intelligent mechatronics, intelligent learning control methods with their applications to intelligent automation, AI robots, smart machinery and smart agriculture.